ARTICLES
PUBLISHED ONLINE: 21 JUNE 2009 | DOI: 10.1038/NPHOTON.2009.96
nature photonics

Increased light harvesting in dye-sensitized solar cells with energy relay dyes

Brian E. Hardin[1,2], Eric T. Hoke[1], Paul B. Armstrong[3], Jun-Ho Yum[2], Pascal Comte[2], Tomás Torres[4], Jean M. J. Fréchet[3], Md Khaja Nazeeruddin[2], Michael Grätzel[2] and Michael D. McGehee[1]*

Conventional dye-sensitized solar cells have excellent charge collection efficiencies, high open-circuit voltages and good fill factors. However, dye-sensitized solar cells do not completely absorb all of the photons from the visible and near-infrared domain and consequently have lower short-circuit photocurrent densities than inorganic photovoltaic devices. Here, we present a new design where high-energy photons are absorbed by highly photoluminescent chromophores unattached to the titania and undergo Förster resonant energy transfer to the sensitizing dye. This novel architecture allows for broader spectral absorption, an increase in dye loading, and relaxes the design requirements for the sensitizing dye. We demonstrate a 26% increase in power conversion efficiency when using an energy relay dye (PTCDI) with an organic sensitizing dye (TT1). We estimate the average excitation transfer efficiency in this system to be at least 47%. This system offers a viable pathway to develop more efficient dye-sensitized solar cells.

Dye-sensitized solar cells (DSCs) work on the basis of light harvesting using a sensitizing dye (SD) attached to a wide-bandgap semiconductor[1–5]. DSCs are composed mainly of abundant, non-toxic materials and offer an inexpensive route to the development of highly efficient photovoltaic cells. State-of-the-art DSCs, which absorb light from 350 to 700 nm, have validated power conversion efficiencies of over 11% (ref. 6). A key to improving the efficiency of DSCs is to increase their spectral absorption range. To reach power conversion efficiencies of 15% using an I^-/I_3^- redox couple, DSCs must absorb ~80% of the solar spectrum from 350 to 900 nm (ref. 7). Light absorption in DSCs is determined by the molar extinction coefficient of the SD, the surface coverage of the dye (dye molecules nm^{-2}), and the total surface area of the oxide film[8]. Films comprising TiO_2 nanoparticles enhance the surface area; 10-μm-thick films have surface areas ×1,000 greater than that of a flat junction. SDs generally pack tightly on the TiO_2 surface with a density of 0.5–1 dye molecules nm^{-2} (ref. 8). The SD has traditionally been made from ruthenium-based complexes (for example, N719 and Z907)[6,9] that have fairly broad absorption spectra ($\Delta\lambda \approx 350$ nm) but low molar extinction coefficients (5,000–20,000 $M^{-1}\,cm^{-1}$). Organic dyes have recently been developed with substantially higher molar extinction coefficients (50,000–200,000 $M^{-1}\,cm^{-1}$) but narrow spectral bandwidths ($\Delta\lambda \approx 250$ nm)[10–13]. As a general rule, dyes that absorb strongly do not typically exhibit broad absorption.

Co-sensitization of titania by dyes with complimentary absorption spectra has been demonstrated to enhance light absorption and broaden the spectral response of organic DSCs (ref. 14). However, the limited number of sites on the titania surface to which dye molecules attach places a constraint on the light absorption achievable by co-sensitization. Furthermore, co-sensitization requires that each dye adsorb strongly on the surface, transfer charge efficiently into the TiO_2 (refs 15–18), have slow recombination (that is, in the millisecond time domain)[17,19–21], and regenerate with the redox couple[22]. Few dyes exist that are both excellent absorbers and possess the requisite energy levels and chemical anchoring groups to be good SDs. A recent study has demonstrated the use of Förster resonant energy transfer (FRET) between covalently linked energy donor molecules to the SD attached on the titania surface[23]. Siegers and colleagues[23] were able to demonstrate a high excitation transfer efficiency (>89%) between attached dye molecules and an improvement in the device external quantum efficiency of 5–10% between 400 and 500 nm. However, the overall power conversion efficiency enhancement of the DSC was low (<9%) and linked more to an increase in the open-circuit voltage rather than an increase in the short-circuit photocurrent density.

In this Article we demonstrate that unattached, highly luminescent chromophores (PTCDI) inside the liquid electrolyte can absorb high-energy photons and efficiently transfer the energy to the anchored near-infrared sensitizing zinc phthalocyanine dye (TT1), increasing the absorption bandwidth of the DSC. Figure 1 shows two routes for charge generation incorporated in this system. In typical DSCs, light is absorbed by the SD (1), which transfers an electron into the titania and a hole into the electrolyte. In the new design, the unattached energy relay dye (ERD) is excited by higher energy (blue) photons and then undergoes Förster energy transfer (2) to the SD. This design is analogous to photosynthesis in purple bacteria, where an aggregate of light-harvesting pigments transfer their energy to the reaction centre, initiating charge separation[24]. In particular, the pigment LH-II is not in direct contact with the reaction centre, and transfers its excitation by means of an intermediate pigment (LH-I) in under 100 ps with ~95% efficiency[25,26].

We recently proposed using unattached ERDs and long-range energy transfer to increase light absorption[27]. Placing the ERDs inside the electrolyte has several important advantages. First, because the attached dye only has to absorb light over a smaller spectral region, it can be chosen to have a stronger and narrower

[1]Department of Material Science and Engineering, Stanford University, Stanford, California, 94305-4045, USA, [2]Laboratoire de Photonique et Interfaces, École Polytechnique Fédérale de Lausanne, CH-1015, Lausanne, Switzerland, [3]Department of Chemistry, University of California, Berkeley, California 94720-1460, USA, [4]Departamento de Química Orgánica (C-I) and Departamento de Física de Materiales (C-IV), Facultad de Ciencias, Universidad Autónoma de Madrid, Cantoblanco, 28049 Madrid, Spain. *e-mail: mmcgehee@stanford.edu

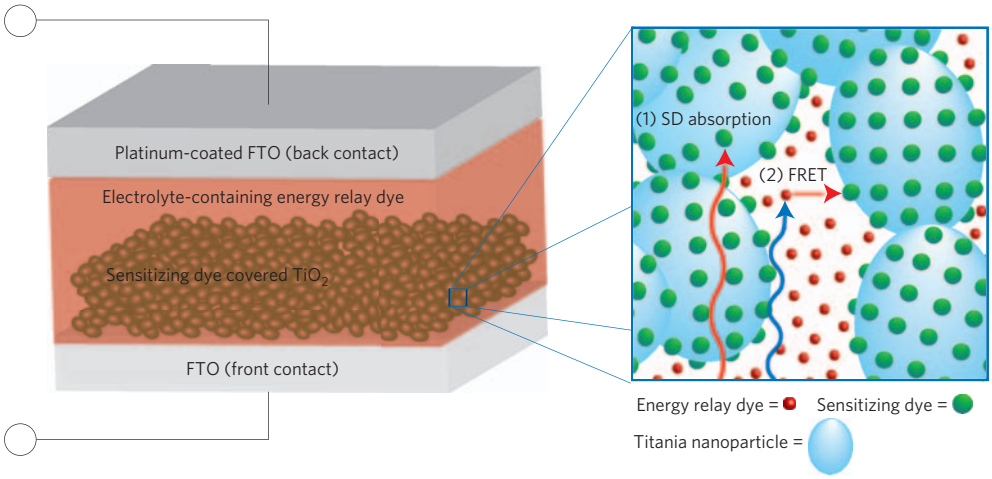

Figure 1 | Schematic representation of a dye-sensitized solar cell (DSC) with energy relay dyes (ERDs). The right side of the figure shows the typical absorption process for lower energy (red) photons in the DSC: light is absorbed by the sensitizing dye (1), transferring an electron into the titania, and a hole is transported to the back contact through the electrolyte. The ERD process is similar, except that higher energy (blue) photons are first absorbed by the ERD, which undergoes Förster energy transfer (2) to the sensitizing dye (SD).

absorption spectrum. Second, the SD can be redshifted compared to the commonly used dyes because the ERD can absorb higher energy photons. Furthermore, it is possible to place multiple ERDs with complementary absorption spectra to tailor light absorption inside the device. Finally, the ERD does not need to be attached to the titania surface and with no additional processing steps can be mixed in very large concentrations inside the electrolyte. In summary, the addition of ERDs into the electrolyte makes the overall absorption spectrum wider and stronger for the same film thickness. It is important to note that the ERDs do not participate in the charge transfer or collection process and thus do not require precise energy levels or specialized attachment groups[28]. ERDs should be designed to be soluble in and not greatly quenched by the electrolyte. The ERD concept is particularly applicable to solid-state DSCs (refs 3,29,30), which are currently restricted to a thickness of 2 μm and are not able to absorb all of the light, even at the peak of the dyes' absorption spectrum. Incorporating long-range energy transfer into the solid-state DSC will require ERDs that avoid charge transfer into the hole transporter. The ERD system is also extremely useful for nanostructured systems (for example, TiO_2 nanotubes[31], ZnO nanorods[32]) that have less available surface area and thus poorer light absorption.

FRET involves dipole–dipole coupling of two chromophores, known as the donor and acceptor, through an electric field[33]. An excitation of the donor, or in our case the ERD, can be transferred non-radiatively through the field to the acceptor, or SD, if there is overlap between the emission spectrum of the donor and the absorption spectrum of the acceptor. Efficient energy transfer over 3–8 nm can be achieved with strong spectral overlap and high donor emission efficiencies, for an isotropic alignment between individual chromophores in solution. If, however, the single acceptor chromophore is replaced by a dense two-dimensional array (that is, SDs tightly packed on the titania surface) FRET can become efficient well over 25 nm from the interface[34,35].

High FRET transfer rates (k_{FRET}) are essential to quickly transfer the energy before the excited ERD non-radiatively decays. The FRET rate is dependent upon the Förster radius (R_o) between the ERD and the SD, the separation distance between the ERD and the SD/TiO_2 interface, which is a function of pore size and geometry, and the natural fluorescence decay rate of the ERD, $k_0 = 1/\tau_0$. The Förster radius, or the distance in which Förster energy transfer is 50% probable between individual chromophores, can be calculated[33] using equation (1):

$$R_o^6 = \frac{9000 \cdot \ln(10)\kappa^2 Q_D}{128 \cdot \pi^5 n^4 N_A} \int F_D(\lambda)\varepsilon_A(\lambda)\lambda^4 \, d\lambda \qquad (1)$$

where n is the index of refraction of the host medium (1.4–1.5 for the DSC electrolyte), κ^2 the orientational factor (2/3 for random orientation), N_A Avogadro's number, Q_D the photoluminescence (PL) efficiency, F_D the emission profile of the donor and $\epsilon(\lambda)$ is the molar extinction coefficient.

A previously reported[36] derivative of perylene-3,4,9,10-tetracarboxylic diimide (PTCDI; Fig. 2b) was synthesized (see Methods) for use as an ERD. PTCDI is an ideal ERD candidate because of its extremely high PL efficiency (>90%), fast fluorescence lifetime (4.8 ns), excellent photo and air stability and relatively strong absorption coefficient (50,000 M^{-1} cm^{-1} at 580 nm)[37] . Its bulky alkyl phenyl substituents were designed to reduce chromophore interactions between adjacent dye molecules in order to prevent aggregate formation and reduction of fluorescence. A zinc phthalocyanine dye (TT1; Fig. 2c) was chosen as the SD for its high molar extinction coefficient of 191,500 M^{-1} cm^{-1} centred at 680 nm (ref. 14). One would prefer a dye with a smaller energy gap, but such dyes are not readily available yet with the necessary anchoring groups. When attached to titania, the TT1 dye absorption broadens (as shown in Fig. 2a) and significantly overlaps the PL emission of the PTCDI. Given the absorption and emission profile of the TT1 and PTCDI, respectively, the Förster radius is estimated to be 8.0 nm. Time-resolved PL measurements on solutions with varying concentration of TT1 determined R_o to be 7.5–7.6 nm (see Supplementary Fig. S1).

Once excited, the ERD can transfer its energy to the SD by means of FRET, emit a photon or non-radiatively decay. Non-radiative decay in the DSC system is greatly increased due to the presence of triiodide in the electrolyte. Triiodide is a highly mobile ion that is known as a 'perfect quencher', meaning that collisions with the ERD have a near unity probability of quenching the excited state[38]. Given the high concentrations of triiodide in the DSC electrolyte, the quenching rate of chromophores can be 20–2,000 times greater than the natural decay rate. Collisional quenching of the PTCDI by triiodide is described by the Stern–Volmer equation (2) (refs 39,40),

$$\frac{PL_0}{PL} = \frac{\tau_0}{\tau} = 1 + k_q \tau_0 [Q] \qquad (2)$$

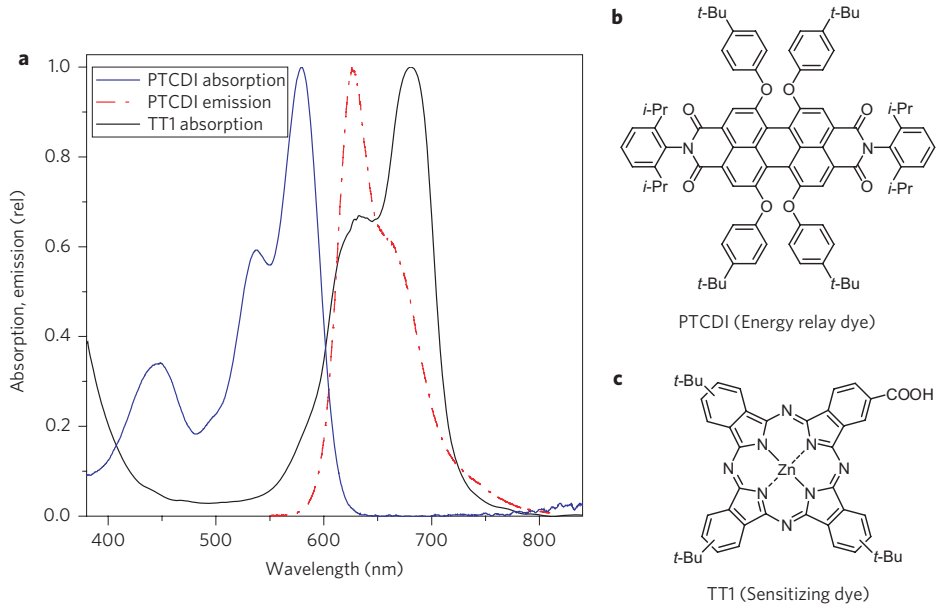

Figure 2 | PTCDI and TT1 properties. a, PTCDI absorption (blue), PTCDI emission (red) in chloroform and TT1 absorption (black) on titania nanoparticles. **b**,**c**, Chemical structures of the energy relay dye PTCDI (**b**), and sensitizing dye TT1 (**c**).

where PL_0 is the photoluminescence in the absence of a quencher, PL the photoluminescence for a given quencher concentration $[Q]$, τ_0 the natural fluorescence lifetime, τ the fluorescence lifetime for a given $[Q]$ and k_q the bimolecular quenching constant, typically around 1×10^9 to 1×10^{10} M^{-1} s^{-1}. Because the bimolecular constant and the electrolyte concentrations are relatively fixed, a short τ_0 is important for minimizing the fluorescence quenching. We determined the fluorescence lifetime of the PTCDI to be 4.8 ns (see Supplementary Fig. S2). Figure 3 shows that the fluorescence intensity and lifetime are both reduced with increasing concentrations of the 1-methyl-3-propyl imidazolium iodide (PMII) and I_2 species with k_q values of 3.17×10^{10} and 0.67×10^{10} M^{-1} s^{-1}, respectively, indicating dynamic quenching. For the electrolyte used in the DSC (0.6 M PMII, 0.05 M I_2) the non-radiative decay rate due to quenching (k_{QUENCH}) is calculated to be ~30 times greater than the natural fluorescence decay rate ($k_{QUENCH} = 30k_0$).

The excitation transfer efficiency (ETE) is the probability that an excited ERD will transfer its energy to a SD. The ETE for a single relay dye molecule at position $\vec{x}$ is dependent on the rate of Förster energy transfer, k_{FRET}, relative to the combined rate of all decay mechanisms including the natural decay rate and quenching rate:

$$\mathrm{ETE}(\vec{x}) = \frac{k_{\mathrm{FRET}}(\vec{x})}{k_0 + k_{\mathrm{QUENCH}} + k_{\mathrm{FRET}}(\vec{x})} \qquad (3)$$

The FRET rate is a function of the separation distance between the ERD molecule and nearby acceptor molecules. The rate of Förster energy transfer between isolated chromophores, known as point-to-point transfer, is given by $k_{FRET} = k_0(R_o)^6/r^6$, where r is the separation distance. When multiple acceptor molecules are present, the FRET rate is equal to the sum of the transfer rates to each of the acceptors. ERDs within the Förster radius of the SD array will transfer their excitation with high efficiency, whereas ERDs in the middle of a large pore may be quenched before energy transfer occurs. We have developed a model that approximates the nanopores as either cylinders or spheres to calculate FRET rate profiles, $k_{FRET}(\vec{x})$, and excitation transfer efficiency profiles, $\mathrm{ETE}(\vec{x})$, using equation (3), and assuming uniform SD coverage over the pore walls. The morphology of the pores has important implications on ERD/SD array separation distance. Assuming a homogeneous ERD concentration,

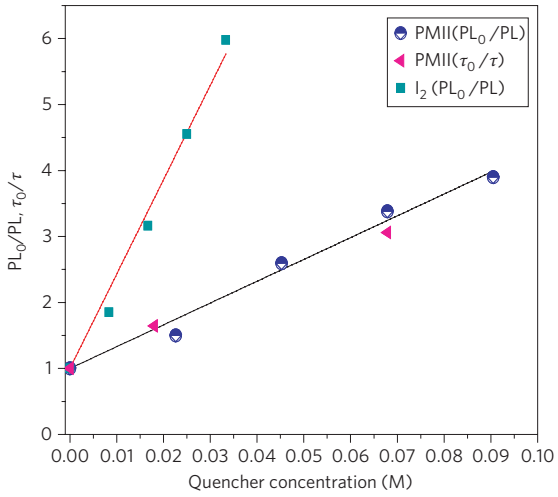

Figure 3 | Quenching of PTCDI by electrolyte species. The PTCDI photoluminescence is reduced with increasing concentration of PMII (half-filled blue circles) and I_2 (green squares). The reduction in photoluminescence (PL_0/PL) by PMII is equivalent to the reduction in excitation lifetime (τ_0/τ) shown as the red triangles. The PTCDI concentration was 1×10^{-4} M in gamma-butyrolactone.

the average separation distance between the ERD and the closest SD/TiO_2 interface in a spherical pore is a quarter of the pore radius, whereas in a cylinder the average separation distance is one-third of the pore radius. Figure 4 shows how the average excitation transfer efficiency, $\overline{\mathrm{ETE}}$, depends on the pore diameter for cylindrical and spherical pores using the parameters calculated for the PTCDI–TT1 DSC system. Although the excited ERD has a non-radiative decay half-life of only 0.15 ns (4.8 ns/31) when placed in the electrolyte, it has an expected $\overline{\mathrm{ETE}}$ between 55 and 70% in a 30 nm pore.

The titania film comprised 20-nm particles to ensure close proximity of the ERD to the SD. The 20-nm TiO_2 particles produce pore diameters between 22 and 38 nm, a film porosity of 68% (without the addition of the dye), and a roughness factor of 97 μm^{-1} (see Supplementary Figs S3,S4). A 10-μm-thick layer of 20-nm particles and a 5-μm-thick layer of 400-nm scattering

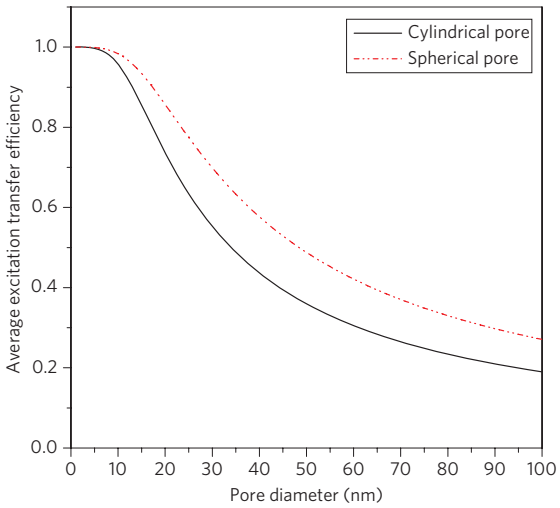

Figure 4 | Modelled average excitation transfer efficiency as a function of pore diameter for spherical and cylindrical pores. Modelling results are based on a Förster radius of 7.5 nm, a measured dye coverage of 0.045 nm^{-2} and a quenching rate of $30k_0$.

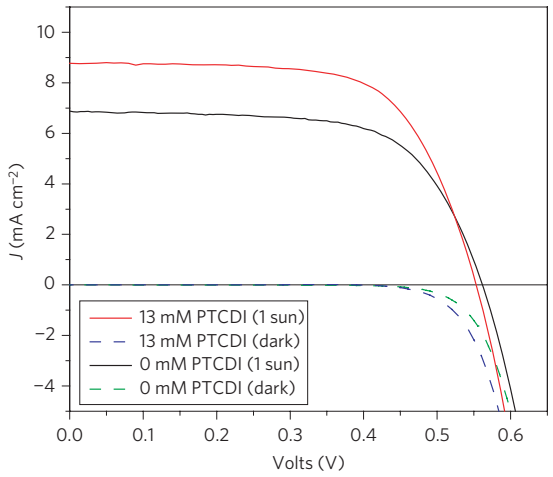

Figure 5 | Photocurrent density–voltage (J–V) characteristics of devices with (13 mM PTGCDI) and without (0 mM PTCDI) energy relay dye (ERD) under AM 1.5G (100 mW cm^{-2}). Dashed lines represent the dark current for the ERD containing DSC (blue) and the control device (green).

particles (CCIC, HPW-400) was formed by means of screen printing, sintered at 450 °C, and subsequently treated in $TiCl_4$ (ref. 41). The films were then dipped in a 1×10^{-5} M solution of TT1 with 10 mM chenodeoxycholic acid for 4 h and rinsed in acetonitrile[42].

Chloroform was chosen as the electrolyte solvent because PTCDI is significantly more soluble in it (>50 mM) compared to commonly used solvents such as acetonitrile (<2 mM) and gamma-butyrolactone (<2 mM). However, chloroform-based electrolytes displayed lower internal quantum efficiency (70% versus 80%) and lower power conversion efficiencies at higher light intensities (see Supplementary Table S1 and Figs S5,S6)[43,44]. These issues are caused by the reduced I_3^- concentration, lower solubility of useful additives such as LiI and guanidinium rhodanide, and the lower dielectric constant of chloroform ($\varepsilon = 5$) compared to acetonitrile ($\varepsilon = 36$)[45–47]. Devices without the ERD were also made with acetonitrile-based electrolytes and had similar device performances compared to the literature (see Supplementary Fig. S7)[14] . The electrolyte contained 0.6 M PMII, 0.05 M I_2, and up to the solubility limits of tertbutyl pyridine (~0.04 M), LiI (~0.01 M) and guanidinium thiocyanate (~0.02 M) in chloroform. PTCDI (13 mM) was subsequently added before electrolyte filling of the DSC. The preparation of the platinum counter-electrode on fluorine-doped tin oxide glass (TEC 15 Ω/□, 2.2 mm thick, Pilkington) is described in a previous report[48]. Electrodes were sealed using a 25-μm-thick hot-melt film (Surlyn 1702, Dupont). A small hole was drilled in the counter-electrode and electrolyte filled using a vacuum pump. It should be noted that $CHCl_3$ has a low boiling point and during electrolyte filling the concentration of PTCDI inside the DSC invariably changed. Higher molar concentrations of PTCDI in the electrolyte did not increase dye loading, but did result in clogging of the hole as the PTCDI electrolyte gelled quickly. A precise determination of the true PTCDI concentration is beyond the scope of this paper, but will be addressed in future publications.

Figure 5 shows the photocurrent density–voltage (J–V) characteristics of DSCs with and without the ERD measured under AM 1.5G (100 mW cm^{-2}) conditions (data shown in Table 1. Devices containing no ERD (0 mM PTCDI) had power conversion efficiencies (PCE) of 2.55% and devices with 13 mM PTCDI had a PCE of 3.21%. The 26% increase in device performance is attributed to the increase in short-circuit photocurrent density (J_{SC}) caused by an increase in the EQE from 400 to 600 nm as shown in Fig. 6a, while the fill factor and open-circuit voltage (V_{OC}) remained relatively unchanged (see Table 1). Devices made with PTCDI but without the SD were found to have very low photocurrent ($J_{SC} <$ 42 μA cm^{-2} and PCE ≈ 0.01%), demonstrating that energy transfer to the SD is necessary for photocurrent generation by the ERD.

A lower bound for EQE of the ERD (EQE_{ERD}) can be calculated from the difference between the EQE of the device containing the ERD and the EQE of the control, ΔEQE, shown in Fig. 6b. The EQE enhancement has a peak of 29.5% at 530 nm, which is ×8 greater than the control (0 mM PTCDI). The ΔEQE spectrum does not perfectly match the absorption of PTCDI because light scattering is greater at lower wavelengths increasing the optical pathway, and at longer wavelengths (>550 nm) the ERD and SD compete for light absorption. The EQE of the ERD is equivalent to the product of the absorption efficiency of the dye, the average excitation transfer efficiency, $\overline{ETE}$, and the internal quantum efficiency (IQE) of the control device:

$$EQE_{ERD} = \eta_{abs,ERD} \cdot \overline{ETE} \cdot IQE \quad (4)$$

A minimum bound for the $\overline{ETE}$ can be calculated by assuming that there is complete light absorption at the ΔEQE peak. Using the dye absorption profiles, this corresponds to $\eta_{abs,ERD} = 89.7\%$ from PTCDI and 10.3% by TT1. If the IQE is assumed to be equal to the peak EQE (70%), a minimum $\overline{ETE}$ of 47% is calculated (see Supplementary Fig. S8).

Using the distribution of pore sizes in the DSC measured by the Brunauer, Emmett and Teller (BET) method (see Supplementary Fig. S4), the measured Förster radius (7.5 nm), the SD surface coverage of 0.045 dye molecules nm^{-2} and the quenching rate calculated above from lifetime measurements ($k_{QUENCH} = 30k_0$) we simulate an $\overline{ETE}$ of 58% for the cylindrical pores and 70% for the spherical pores. This is consistent with the minimum possible ETE observed from the EQE data.

Table 1 | PV characteristics.

	13 mM PTCDI	0 mM PTCDI	Change (%)
J_{SC} (mA cm^{-3})	8.78	6.88	28
V_{OC} (mV)	553	562	−1.60
Fill factor	0.66	0.65	−1.50
PCE (%)	3.21	2.55	26

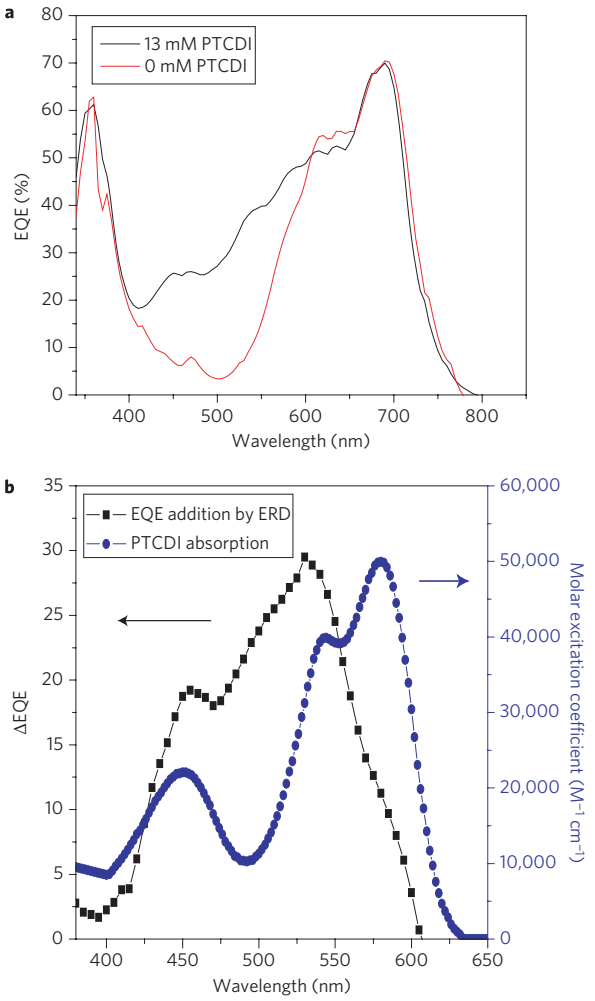

Figure 6 | Light harvesting characteristics of the energy relay dye (ERD) dye-sensitized solar cell (DSC). a, External quantum efficiency (EQE) versus wavelength of the DSC with ERD (PTCDI) and a control device (0 mM PTCDI). **b**, EQE addition (black squares) caused by FRET from the ERD to the sensitizing dye (SD) and PTCDI absorption (blue circles). The peak ΔEQE generated by PTCDI was 29.5% at 530 nm.

It is possible to increase the $\overline{ETE}$ by reducing the average pore size inside the titania film. The ETE can be greater than 90% when using smaller nanoparticles (for example, 14 nm) assuming a SD surface concentration of the SD is 0.2 dye molecules nm^{-2} and a spherical pore geometry. Initial results using 14-nm nanoparticles indicate >69% ETE when using PTCDI with TT1; however, more rigorous analysis is necessary both in determining the exact concentration of PTCDI inside the film and the porosity of the samples with the inclusion of the SD. Incorporating PTCDI derivatives that are soluble in acetonitrile or gamma-butyrolactone into films that contain smaller pores should allow PCEs exceeding 5.5% for the PTCDI/TT1 system (see Supplementary Fig. S9). If multiple relay dyes that have complementary absorption spectra are incorporated into the system, higher PCEs are possible.

Given the predicted $\overline{ETE}$, the development of DSCs with PCEs greater than 15% is possible by using a series of ERDs that absorb light from 350 to 800 nm and an SD that absorbs from 800 to 1,000 nm. The realization of extremely efficient DSCs will require the research and development of SDs that can absorb strongly in the infrared. Future infrared SDs will not be required to absorb as broadly, and because the Förster radius is dependent on the emission/absorption overlap multiplied by the wavelength to the fourth power (λ^4 in equation (1)), it may not need to absorb as strongly. However, the SD will need to have excellent charge injection properties. The potential difference required between the HOMO of the SD and the Nernst potential of the electrolyte is ~300 meV for the iodide/triiodide redox couple and 100–200 meV for the solid-state hole conductor to regenerate the dye. There are many available fluorophores including quantum dots currently used for biomedical imaging that have the potential to be used as ERDs[38], and it may be possible to design ERDs that are minimally quenched by triiodide. Candidates for ERDs should be fast emitters (<100 ns) to reduce quenching by the triiodide and have moderately high PL quantum efficiency (>20%).

Methods

Materials synthesis. All glassware was dried overnight in an oven or by flame before use. Reactions were carried out under nitrogen using standard Schlenk techniques. Reactions were monitored by thin-layer chromatography using Whatman® 250-μm silica gel plates. Flash column chromatography was performed using Merck silica gel, 230–400 mesh. Solvents were removed with a rotary evaporator at aspirator pressure. All reagents were used as received from commercial suppliers without further purification. 9(10),16(17),23(24)-tri-*tert*-butyl-2-carboxy-5,28:14,19-diimino-7,12:21,26 dinitrilotetrabenzo[*c,h,m,r*]tetraazacycloeicosinator-(2⁻)-N^{29},N^{30},N^{31},N^{32} zinc (II) (TT1) was made by a previously reported procedure (ref. 14).

NMR spectra were recorded in $CDCl_3$ with a TMS standard using a Bruker AVB-400 spectrometer. ^{13}C NMR was recorded at 100 MHz using ^1H decoupling. Mass spectrometry and elemental analysis data were recorded by staff members at the UC Berkeley mass spectrometry facility.

Procedure for *N,N′*-di(2,6-diisopropylphenyl)-1,6,7,12-tetra(4-*tert*-butyl phenyoxy)-perylene-3,4,9,10-tetracarboxylic diimide (PTCDI). A solution of *N,N′*-di(2,6-diisopropylphenyl)-1,6,7,12-tetrachloroperylene-3,4,9,10-tetracarboxylic diimide (3.00 g, 3.54 mmol, procedure from ref. 49), 4-*tert*-butylphenol (2.66 g, 17.7 mmol), and potassium carbonate (2.92 g, 17.7 mmol) in anhydrous *N*-methylpyrrolidinone (50 ml) was stirred at 130 °C for 16 h. The solution was rapidly poured into 1 M HCl (200 ml) and the resulting precipitate isolated by vacuum filtration and washed repeatedly with water. The precipitate was dissolved in chloroform and extracted twice with water. The chloroform layer was then dried over Na_2SO_4 and concentrated. Purification by flash column chromatography (eluent: 40–55% dichloromethane in hexanes) yielded 1.55 g of red solid (34% yield). A portion of this product was further purified by recrystallization: 1.00 g of product was dissolved in dichloromethane (100 ml) and placed in a 1,000 ml graduated cylinder. Methanol (200 ml) was carefully layered on top of the dichloromethane, and the two layers were allowed to mix slowly over 1 week. The resulting red crystals were isolated by filtration and dried under vacuum, yielding 740 mg of red product.

Characterization. m.p. > 300 °C. ^1H NMR (400 MHz, $CDCl_3$, δ): 8.29 (s, 4H), 7.42 (t, J = 7.8 Hz, 2H), 7.22–7.28 (m, 12H), 6.87 (dt, J = 8.8 and 2.5 Hz, 8H), 2.71 (m, J = 6.8 Hz, 4H), 1.28 (s, 36H), 1.13 (d, J = 6.8 Hz, 24H). ^{13}C NMR (100 MHz, $CDCl_3$, δ): 163.55, 156.12, 152.99, 147.55, 145.82, 133.44, 130.88, 129.60, 126.88, 124.09, 122.89, 120.97, 120.45, 120.39, 119.41, 34.58, 31.66, 29.28, 24.24. FTIR (film on NaCl): ν = 2,963, 2,870, 1,709, 1,675, 1,588, 1,505, 1,406, 1,340, 1,285, 1,209, 1,175 cm^{-1}. HRMS (FAB+, *m/z*): calculated for $C_{88}H_{91}N_2O_8$, 1303.6775; found, 1303.6786. Anal. calculated for $C_{88}H_{90}N_2O$: C 81.07, H 6.96, N 2.15; found: C, 80.08; H, 6.97; N, 2.09.

Electrical measurements. The power of the AM 1.5 solar simulator (100 mW cm^{-2}) was calibrated using a reference silicon photodiode equipped with an infrared cutoff filter (KG-3, Schott) to reduce the mismatch between the simulated light and solar spectrum from 350–700 nm to less than 2% (ref. 50). The *J–V* curves were obtained by externally biasing the DSC and measuring the photocurrent using a Keithley 2400 digital source meter. All measurements were performed using a metal mask with an aperture of 0.159 cm^2 to reduce light scattering.

The EQE measurement light source was a 300 W xenon lamp (ILC Technology), which was focused through a Gemini-180 double monochromator (Jobin Yvon). EQE measurements were performed at 1% sun using a metal mask with an aperture area of 0.159 cm^2. Integrating the EQE spectra of the ERD-containing and control DSCs resulted in slightly higher (~10%) estimated J_{SC} at full sun than those measured in the devices. This is a result of charge transport limitations caused by the electrolyte at higher light intensities. Extrapolating device results from measurements taken at 10% sun (see Supplementary Fig. S6) to full sun are consistent with the estimated J_{SC} from the EQE results. The difference in the integrated EQE spectrum between the ERD-containing and control devices is the same ratio as the differences in J_{SC} at full sun.

Photoluminescence lifetime measurements. Time-resolved PL measurements were performed using a time-correlated single-photon counting (TCSPC) system from PicoQuant. Solutions were excited with a pulsed laser diode, (model LDH 485: 481 nm, 70 ps FWHM, 5 MHz) detected with a single-photon avalanche diode

(PDM 100CT SPAD) attached to a monochromator and processed by a PicoHarp 300 correlating system.

Received 12 March 2009; accepted 18 May 2009; published online 21 June 2009

References

1. O'Regan, B. & Gratzel, M. A low-cost, high-efficiency solar cell based on dye-sensitized colloidal TiO_2 films. *Nature* **353,** 737–740 (1991).
2. Peter, L. M. Dye-sensitized nanocrystalline solar cells. *Phys. Chem. Chem. Phys.* **9,** 2630–2642 (2007).
3. Snaith, H. J. & Schmidt-Mende, L. Advances in liquid-electrolyte and solid-state dye-sensitized solar cells. *Adv. Mater.* **19,** 3187–3200 (2007).
4. Bisquert, J., Cahen, D., Hodes, G., Ruhle, S. & Zaban, A. Physical chemical principles of photovoltaic conversion with nanoparticulate, mesoporous dye-sensitized solar cells. *J. Phys. Chem. B* **108,** 8106–8118 (2004).
5. Hagfeldt, A. & Gratzel, M. Molecular photovoltaics. *Acc. Chem. Res.* **33,** 269–277 (2000).
6. Nazeeruddin, M. K. *et al.* Combined experimental and DFT-TDDFT computational study of photoelectrochemical cell ruthenium sensitizers. *J. Am. Chem. Soc.* **127,** 16835–16847 (2005).
7. Hamann, T. W., Jensen, R. A., Martinson, A. B. F., Ryswyk, H. V. & Hupp, J. T. Advancing beyond current generation dye-sensitized solar cells. *Energy Environ. Sci.* **1,** 66–78 (2008).
8. Gratzel, M. Conversion of sunlight to electric power by nanocrystalline dye-sensitized solar cells. *J. Photochem. Photobiol. A* **164,** 3–14 (2004).
9. Wang, P. *et al.* A stable quasi-solid-state dye-sensitized solar cell with an amphiphilic ruthenium sensitizer and polymer gel electrolyte. *Nature Mater.* **2,** 402–407 (2003).
10. Yum, J.-H. *et al.* Efficient far red sensitization of nanocrystalline TiO_2 films by an unsymmetrical squaraine dye. *J. Am. Chem. Soc.* **129,** 10320–10321 (2007).
11. Burke, A., Schmidt-Mende, L., Ito, S. & Gratzel, M. A novel blue dye for near-IR 'dye-sensitized' solar cell applications. *Chem. Commun.* **3,** 234–236 (2006).
12. Campbell, W. M. *et al.* Highly efficient porphyrin sensitizers for dye-sensitized solar cells. *J. Phys. Chem. C* **111,** 11760–11762 (2007).
13. He, J. *et al.* Modified phthalocyanines for efficient near-IR sensitization of nanostructured TiO_2 electrode. *J. Am. Chem. Soc.* **124,** 4922–4932 (2002).
14. Cid, J.-J. *et al.* Molecular cosensitization for efficient panchromatic dye-sensitized solar cells. *Angew. Chem.* **119,** 8510–8514 (2007).
15. Tachibana, Y., Nazeeruddin, M. K., Grätzel, M., Klug, D. R. & Durrant, J. R. Electron injection kinetics for the nanocrystalline TiO_2 films sensitised with the dye $(Bu_4N)_2Ru(dcbpyH)_2(NCS)_2$. *Chem. Phys.* **285,** 127–132 (2002).
16. Tachibana, Y., Moser, J. E., Gratzel, M., Klug, D. R. & Durrant, J. R. Subpicosecond interfacial charge separation in dye-sensitized nanocrystalline titanium dioxide films. *J. Phys. Chem.* **100,** 20056–20062 (1996).
17. Haque, S. A. *et al.* Parameters influencing charge recombination kinetics in dye-sensitized nanocrystalline titanium dioxide films. *J. Phys. Chem. B* **104,** 538–547 (2000).
18. Nazeeruddin, M. K. *et al.* Conversion of light to electricity by *cis*-X_2*bis*(2,2′-bipyridyl-4,4′-dicarboxylate)ruthenium(II) charge-transfer sensitizers (X = Cl^-, Br^-, I^-, CN^- and SCN^-) on nanocrystalline titanium dioxide electrodes. *J. Am. Chem. Soc.* **115,** 6382–6390 (1993).
19. Haque, S. A., Tachibana, Y., Klug, D. R. & Durrant, J. R. Charge recombination kinetics in dye-sensitized nanocrystalline titanium dioxide films under externally applied bias. *J. Phys. Chem. B* 1998, 1745–1749 (1998).
20. O'Regan, B. C. *et al.* Catalysis of recombination and its limitation on open circuit voltage for dye sensitized photovoltaic cells using phthalocyanine dyes. *J. Am. Chem. Soc.* **130,** 2906–2907 (2008).
21. O'Regan, B. C. *et al.* Structure/function relationships in dyes for solar energy conversion: a two-atom change in dye structure and the mechanism for its effect on cell voltage. *J. Am. Chem. Soc.* **131,** 3541–3548 (2009).
22. Clifford, J. N., Palomares, E., Nazeeruddin, M. K., Gratzel, M. & Durrant, J. R. Dye dependent regeneration dynamics in dye sensitized nanocrystalline solar cells: Evidence for the formation of a ruthenium bipyridyl cation/iodide intermediate. *J. Phys. Chem. C* **111,** 6561–6567 (2007).
23. Siegers, C. *et al.* A dyadic sensitizer for dye solar cells with high energy-transfer efficiency in the device. *Chem. Phys. Chem.* **8,** 1548–1556 (2007).
24. Hu, X. & Schulten, K. How nature harvests sunlight. *Phys. Today* **50,** 28–34 (1997).
25. Hu, X., Damjanovic, A., Ritz, T. & Schulten, K. Architecture and mechanism of the light-harvesting apparatus of purple bacteria. *Proc. Natl Acad. Sci. USA* **95,** 5935–5941 (1998).
26. Pullerits, T. & Sundstrom, V. Photosynthetic light-harvesting pigment–protein complexes: Toward understanding how and why. *Acc. Chem. Res.* **29,** 381–389 (1996).
27. Hardin, B. E. in *et al.* Materials Research Society Fall Meeting (Boston, MA, 2008).
28. Siegers, C. *et al.* Overcoming kinetic limitations of electron injection in the dye solar cell via coadsorption and FRET. *Chem. Phys. Chem.* **9,** 793–798 (2008).
29. Bach, U. *et al.* Solid-state dye-sensitized mesoporous TiO_2 solar cells with high photon-to-electron conversion efficiencies. *Nature* **395,** 583–585 (1998).
30. Snaith, H. J. *et al.* Efficiency enhancements in solid-state hybrid solar cells via reduced charge recombination and increased light capture. *Nano Lett.* **7,** 3372–3376 (2007).
31. Mor, G. K., Shankar, K., Paulose, M., Varghese, O. K. & Grimes, C. A. Use of highly-ordered TiO_2 nanotube arrays in dye-sensitized solar cells. *Nano Lett.* **6,** 215–218 (2006).
32. Law, M., Greene, L. E., Johnson, J. C., Saykally, R. & Yang, P. Nanowire dye-sensitized solar cells. *Nature Mater.* **4,** 455–459 (2005).
33. Forster, T. Transfer mechanisms of electronic excitation. *Discuss. Faraday Soc.* **27,** 7 (1959).
34. Scully, S. R., Armstrong, P. B., Edder, C., Frechet, J. M. J. & McGehee, M. D. Long-range resonant energy transfer for enhanced exciton harvesting for organic solar cells. *Adv. Mater.* **19,** 2961–2966 (2007).
35. Liu, Y. X., Summers, M. A., Edder, C., Fréchet, J. M. J. & McGehee, M. D. Using resonance energy transfer to improve exciton harvesting in organic–inorganic hybrid photovoltaic cells. *Adv. Mater.* **17,** 2960–2964 (2005).
36. Hill, Z. B., Rodovsky, D. B., Leger, J. M. & Bartholomew, G. P. Synthesis and utilization of perylene-based n-type small molecules in light-emitting electrochemical cells. *Chem. Commun.* 6594–6596 (2008).
37. Wurthner, F. Perylene bisimide dyes as versatile building blocks for functional supramolecular architectures. *Chem. Commun.* 1564–1579 (2004).
38. Lakowicz, J. R. *Principles of Fluorescence Spectroscopy* (Plenum, 1999).
39. Stern, V. O. & Volmer, M. Uber die abklingungszeit der fluoreszenz. *Zeitschrift für Physik* **20,** 183–189 (1919).
40. Mac, M., Wach, A. & Najbar, J. Solvents effects on the fluorescence quenching of anthracene by iodide ions. *Chem. Phys. Lett.* **176,** 167–172 (1991).
41. Sommeling, P. M. *et al.* Influence of a $TiCl_4$ post-treatment on nanocrystalline TiO_2 films in dye-sensitized solar cells. *J. Phys. Chem. B* **110,** 19191–19197 (2006).
42. Yum, J.-H. *et al.* Effect of coadsorbent on the photovoltaic performance of zinc pthalocyanine-sensitized solar cells. *Langmuir* **24,** 5636–5640 (2008).
43. Haque, S. A. *et al.* Charge separation versus recombination in dye-sensitized nanocrystalline solar cells: the minimization of kinetic redundancy. *J. Am. Chem. Soc.* **127,** 3456–3462 (2005).
44. Huang, S., Schlichthorl, G., Nozik, A., Gratzel, M. & Frank, A. Charge recombination in dye-sensitized nanocrystalline TiO_2 solar cells. *J. Phys. Chem. B* **101,** 2576–2582 (1997).
45. Kebede, Z. & Lindquist, S.-E. Donor–acceptor interaction between non-aqueous solvents and I_2 to generate I_3^-, and its implication in dye sensitized solar cells. *Solar Energy Mater. Solar Cells* **57,** 259–275 (1999).
46. Fabregat-Santiago, F., Bisquert, J., Garcia-Belmonte, G., Boschloo, G. & Hagfeldt, A. Influence of electrolyte in transport and recombination in dye-sensitized solar cells studied by impedance spectroscopy. *Solar Energy Mater. Solar Cells* **87,** 117–131 (2005).
47. Haque, S. A. *et al.* Charge separation versus recombination in dye-sensitized nanocrystalline solar cells: The minimization of kinetic redundancy. *J. Am. Chem. Soc.* **127,** 3456–3462 (2005).
48. Ito, S. *et al.* Fabrication of thin film dye sensitized solar cells with solar to electric power conversion efficiency over 10%. *Thin Solid Films* **516,** 4613–4619 (2008).
49. Klok, H. A., Hernández, J. R., Becker., S. & Müllen, K. Star-shaped fluorescent polypeptides. *J. Polym. Sci. Part A: Polym. Chem.* **39,** 1572–1583 (2001).
50. Ito, S. *et al.* Calibration of solar simulator for evaluation of dye-sensitized solar cells. *Solar Energy Mater. Solar Cells* **82,** 421–429 (2004).

Acknowledgements

The authors thank Y.C. Jun and M.L. Brongersma for access to time-resolved PL measurement equipment and assistance with measurements. B.E.H. would like to thank P. Péchy for his assistance in making the electrolyte. This work was supported by the King Abdullah University of Science and Technology Center for Advanced Molecular Photovoltaics and by the Office of Naval Research contract no. N00014-08-1-1163. B.E.H. received financial support from the National Department of Defense Science and Engineering Graduate Fellowship (NDSEG). E.T.H. is supported by the National Science Foundation GRFP and the Fannie and John Hertz Foundation. J.M.F. is supported by DOE-BES contract DE-AC02-05CH11231.

Author contributions

B.E.H. assembled the DSCs and performed measurements for Figs 3, 5 and 6. E.T.H. modelled the excitation transfer efficiency for the spherical and cylindrical geometries shown in Fig. 4. P.B.A. synthesized the ERD (PTCDI) and T.T. synthesized the sensitizing dye (TT1). P.C. fabricated the TiO_2 electrodes and provided BET data to determine pore size. J.Y.H. and M.K.N. measured dye absorption and dye adsorption on TiO_2 and provided guidance in electrolyte design. J.M.J., M.G. and M.D.M. provided technical advice on dye design and DSC device physics.

Additional information

Supplementary information accompanies this paper at www.nature.com/naturephotonics. Reprints and permission information is available online at http://npg.nature.com/reprintsandpermissions/. Correspondence and requests for materials should be addressed to M.D.M.